UNIVERSITY OF CALIFORNIA,
IRVINE

Use of Computational Fluid Dynamic Simulation to assess the effects of Nitric Oleic Acid on Methyl Isocyanate treated Rat Tracheas

THESIS

submitted in partial satisfaction of the requirements
for the degree of

MASTER OF SCIENCE

in ENGINEERING

by

Andy Choi

Thesis Committee:
Professor Zhongping Chen, Chair
Professor William Tang
Assistant Professor Michelle Digman

2019

DEDICATION

I would like to dedicate this work to my loving mother, Sandra Liu, who always pushed me to be my best even when life didn't give me the best opportunities. Thank you for being such a strong single mother and being able to raise me into who I am today.

TABLE OF CONTENTS

	Page
LIST OF FIGURES	iv
ACKNOWLEDGMENTS	v
ABSTRACT OF THE THESIS	vi
INTRODUCTION	1
CHAPTER 1: Methyl Isocyanate	1
Nitro Oleic Acid	2
Optical Coherence Tomography	3
CHAPTER 2: Collecting OCT Images of Trachea	4
Reconstruction of Airway from OCT Images	6
Preparing Model for Simulation	8
Turbulent vs Laminar Flow	10
Assumptions and Model Parameters	11
CHAPTER 3: Cross-sectional Area of Trachea	14
Velocity Across Rat Trachea	14
Pressure Drop Across Rat Trachea	20
Airway Resistance Across	26
CHAPTER 4: Summary and Conclusions	28
REFERENCES (OR BIBLIOGRAPHY)	30

LIST OF FIGURES

		Page
Figure 1	Basic schematic of OCT system	3
Figure 2	Probe used to image rat tracheas	5
Figure 3	Images of MIC healthy and diseased rat tracheas	6
Figure 4	Outline of using OCT images to create volumes	8
Figure 5	Image of flat ends used as outlet/inlet	9
Figure 6	Cells generated by ANSYS	9
Figure 7	Effects of inflation on trachea models	10
Figure 8	Graph of each group's average Reynold's number	11
Figure 9	Image of sliced model created to extract information	13
Figure 10	Average cross-sectional area of trachea	14
Figure 11	Average airway velocity of each trachea	15
Figure 12	Images of velocity simulation results	16-19
Figure 13	Average pressure drop graph	20
Figure 14	Images of pressure simulation results	22-25
Figure 15	Airway resistance graph	27

ACKNOWLEDGMENTS

I would like to thank the people who have helped me through my academic journey and given me a chance to better myself as an individual.

To my professor Zhongping Chen, I would like to thank him for giving me the chance to study an interesting and exciting technology. He gave me an opportunity to expand my knowledge and hone my skills on interesting and challenging projects that made me a better engineer.

To the Henry Samueli School of Engineering faculty who provided an excellent learning environment that stimulated learning and discovery: all of the professors have a true zeal for their area of interest and are always a wealth of knowledge which is made available to all students.

And finally, to the members of the F-OCT lab who have been always helpful whenever I would have questions or needed help with any part of the lab. In particular, I would like to thank Yusi Miao, Jason Chen, and Yan Li who never hesitated to take time out of their busy schedules to help me.

ABSTRACT OF THE THESIS

Belief Revision and Machine Discovery

By

Andy Choi

Master of Science

University of California, Irvine

2019

Professor Zhongping Chen, Chair

Methyl Isocyanate has been known to be a very toxic and it can lead to many different chronic respiratory diseases if left untreated. Despite the potential impact on public health, no effective counteragents have been discovered. Recently, several studies showed administration of Nitro Oleic Acid can reverse the effects of Methyl Isocyanate. In this study, we aim to test the effectiveness of the treatment to improve airway obstruction using a minimally-invasive optical coherence tomography (OCT) endoscopy and computational fluid dynamics (CFD) analysis. Rats were first exposed to Methyl Isocyanate and treated with different levels of Nitro Oleic Acid. Immediately after the animals were sacrificed, OCT images of the tracheas were taken to create a 3D reconstruction of the trachea. Finally, computational fluid dynamics simulations were performed to investigate how air would flow through the trachea and measured the performance of the trachea based on velocity, cross-sectional area, pressure, and airway resistance. We found the rats treated with Methyl Isocyanate only performed the worst while the 30 mg NO_2OA treated rats were closer to healthy levels based on the OCT measurements and flow simulation results.

1. INTRODUCTION

1.1 Methyl Isocyanate

Methyl Isocyanate (MIC) is a colorless liquid that is known to create an exothermic reaction creating carbon dioxide, methylamine gases, and N-Dimethyl urea. These toxic gases are known to cause respiratory system damage with symptoms such as breathlessness, coughing, throat irritation or choking, chest pains, and hemoptysis being the most common. One of the more recent tragedies involving this gas was the Bhopal incident on December 3, 1984. The chemical was imported from the United States and used to create pesticides on site where the incident occurred. The accident occurred when tank 610, which carried approximately 40,900 kg of MIC, was exposed to water and caused an exothermic reaction to occur and released the toxic gases as far as 8 km away from the factory. It is estimated that nearly 200,000 people were affected by the gas with 2,500 to 5,000 people dying due to the exposure [1].

After the tragedy at Bhopal, the severity of MIC exposure was evaluated using rats. Nemery et al. exposed six male LAC-P rats to varying concentrations of MIC to determine the detrimental effects on the respiratory system. Exposing the rats to moderate to lethal amounts of MIC (0.1, 0.25, 0.5, and 1mg/l) caused detachment of epithelial cells from the basement membrane. The cells exposed to the gas began undergoing necrosis with large areas of the respiratory tract missing epithelial cells. After three weeks, most of the epithelium damage from the gas exposure had been repaired in the rats, but alveolar hemorrhage and groups of necrotic cells were still present [2].

1.2 Nitro Oleic Acid

One novel possible treatment that has emerged is the use of a drug called Nitro Oleic Acid (NO_2OA). NO_2OA is a derivative of nitro-fatty acids (NO_2FA), which is formed during digestion and responsible for regulating metabolic and inflammatory signaling, cell signaling, and gene expression responses. NO_2OA has been shown to have cyto-protective properties while also acting as an anti-inflammatory when it is present. The drug was used on MIC treated rats to see if the effects of MIC exposure could be reversed back to an acceptable level [3]. Other groups have demonstrated the advantages of this drug in the case of ventral hernia repair with an elastomeric polyester carbonate urethane urea matrix loaded with microspheres of NO_2OA. The first benefit shown from the inclusion of NO_2OA in the scaffold is the reduction of scar tissue 8 weeks after the scaffold is placed within the herniated rat abdomen. With just the scaffold, the percentage of collagen present indicated scar tissue averaged 23%, but with the scaffold and an extracellular matrix layer, the collagen percentage dropped to an average of 13. With the inclusion of NO_2OA in the scaffold and ECM matrix, the collagen percentage dropped even further to a 7 percent average which shows NO_2OA does help with tissue repair. The thickness of the tissue also improved substantially with the scaffold group having a 0.5mm thickness: the scaffold and ECM group had a thickness of 0.8mm, and the scaffold, ECM, and NO_2OA group had a thickness of 1.2mm. The same pattern was also seen in blood vessel development with the scaffold having the lowest density with 10 vessels/mm^2. The scaffold and ECM group had a density of 20 vessels/mm^2, and the scaffold, ECM, and NO_2OA group had the highest vessel density of 38 vessels/mm^2. Overall, NO_2OA has been shown to have a positive effect when used for tissue repair and could be applied to other areas of the body [4].

1.3 Optical Coherence Tomography

Optical Coherence Tomography (OCT) is a novel imaging technology that is able to produce high resolution cross-sectional images of living tissues (fig 1). In order to achieve these high-resolution images, OCT emits a broadband laser on an object, and the backscattered light from the object is recorded. In order to get a clearer image, the backscattered light is then superimposed on the original laser pulse in order to amplify the intensity of the interference pattern. This creates a situation where two arms are used with the reference arm being the laser shot at the mirror and the sample arm which is aimed at the sample that is being imaged. A beam splitter is used to separate the laser pulse and recombine the light once it has been reflected from the aimed target [5].

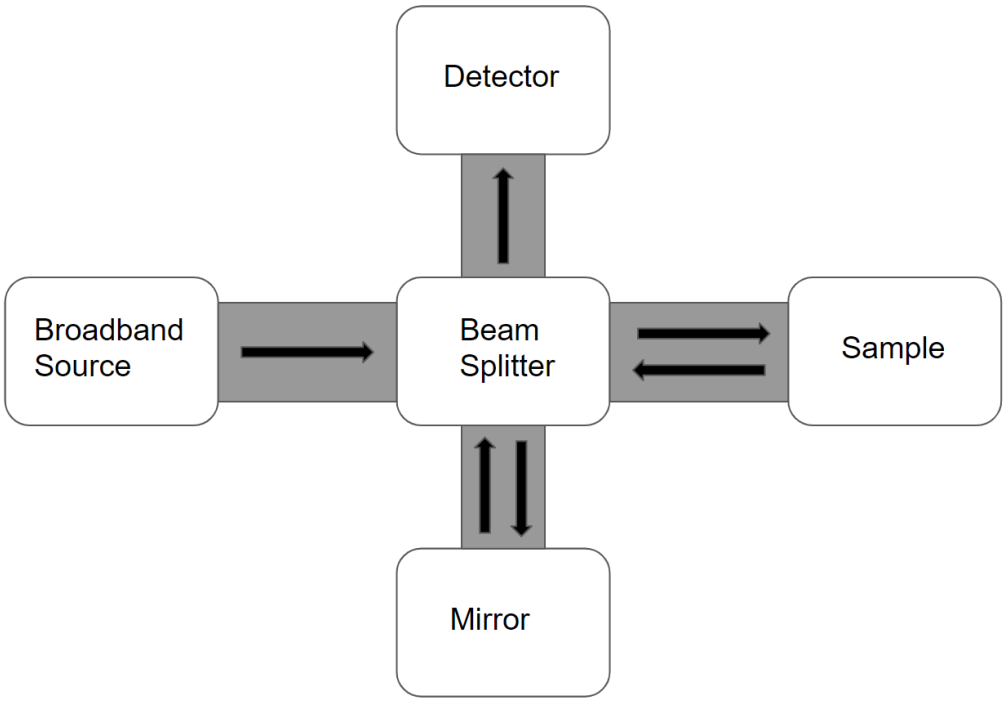

Figure 1 - Basic schematic of an OCT system. Light originates at the source where the light is split by the beam splitter into the sample and mirror. The backscatter from the sample and the reflected light from the mirror are then read by the detector after the light passes through the beam splitter again [5].

2. MATERIALS AND METHODS

2.1 Collecting OCT Images of Trachea

In order to image the trachea of a rat, an endoscopic probe that is small enough to fit down the length of the trachea needed to be developed (fig. 2). The probe needed to be flexible and small enough to fit down the obstructed tracheas and be able to side scan in order to achieve 3D volumetric imaging. The probe was created from three different diameter cores of 9, 12, and 20 um to reduce the divergence of light and increase lateral resolution of the probe. Due to the relatively small trachea diameter of a healthy rat (2.8 mm), a focusing lens was not needed to get images of the wall. For a human trachea, a probe of 1.2mm in diameter is normally used, but for this newly designed probe, a diameter of 0.4mm was achieved. The probe was sheathed in two layers with a metal housing placed on the outside of the probe in order to reduce friction and then another 24-gauge optically transparent sheath covered the entire probe to ensure the probe would not be damaged during imaging. The probe was rotated at 1,500 rpm and acquired images at a rate of 25 frames per second. The probe was pulled back at a rate of 5 mm/s with a linear stage with a power emission of 5.8 mW. The OCT system was based on Fourier domain OCT and used a 50 kHz swept-source laser with a 1310 wavelength and a bandwidth of 110 nm. The laser was split by a 90/10 coupler for the sample and reference arm, respectively. The reflected light was returned to the detector by a 50/50 coupler with the detector being a 1.6 GHz wide balanced detector. The system sensitivity was recorded to be 102 dB.

The Methyl Isocyanate was synthesized by MRIGLobal using the Curtius Rearrangement method by refluxing acetyl chloride with sodium azide in toluene until the Methyl Isocyanate was produced [6]. The gas was 99.2% pure after testing it using

chromatography-flame ionization detection. Images of the rat trachea were taken ex vivo with the respiratory system left with both the airway and lungs intact within the rat after euthanasia. The rats were kept in iced saline-soaked gauze and imaged as soon as possible after they were euthanized. The probe was inserted into the anterior nasal airway where it was carefully placed down the airway until the probe was placed at the distal end of the carina (fig 3). To get a volumetric image of the entire trachea, the system would need 15 seconds to pull back. Images of a healthy trachea, a MIC exposed trachea and two healthy tracheas were acquired [7].

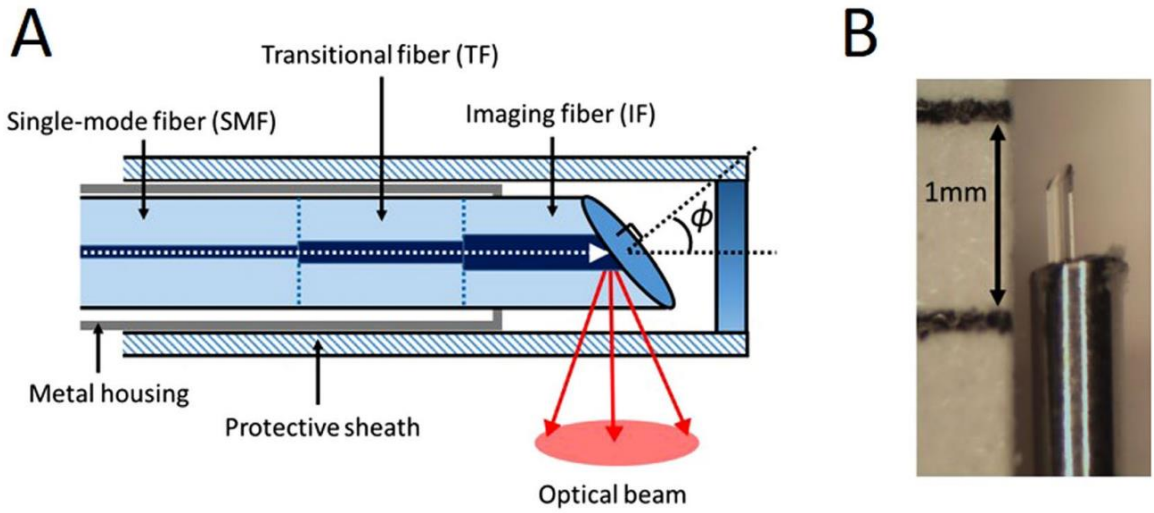

Figure 2 - A. The probe made from the three different fiber cores. B. The 0.4mm probe with the fiber [7].

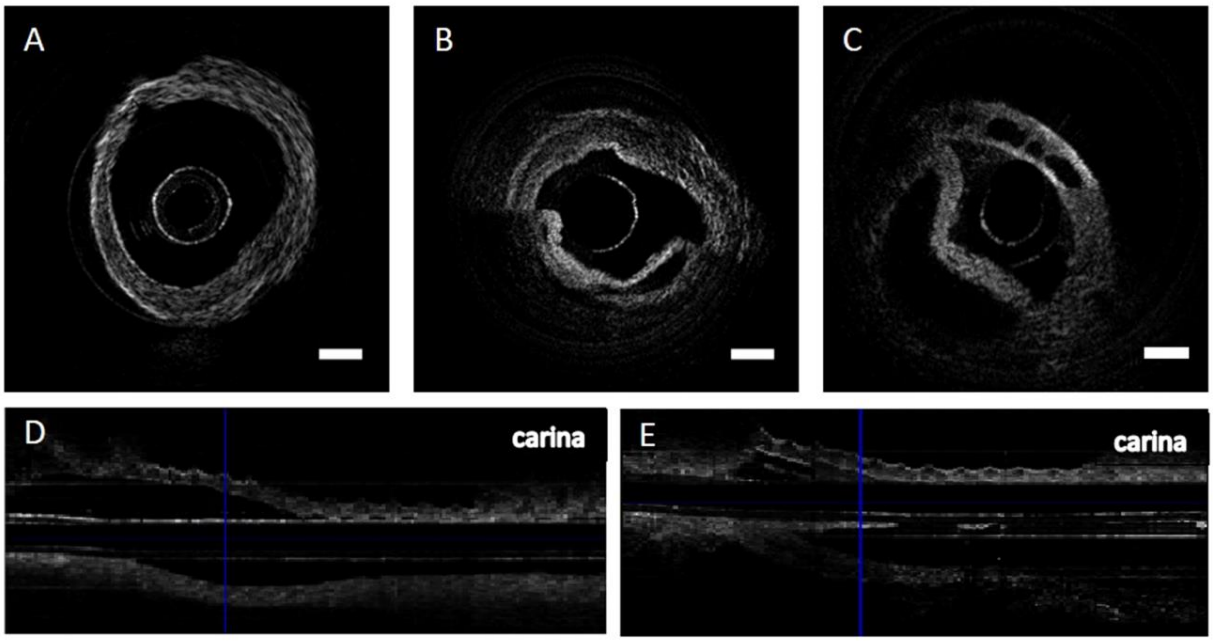

Figure 3 - A. Image of an MIC exposed rat trachea where tissue detachment and sloughing has occurred. B. Image of another MIC rat with air pockets in airway wall. C. Image of normal rat trachea. D and E. Longitudinal images of MIC exposed tracheas with the blue line indicating the obstruction [7].

2.2 Reconstruction of Airway from OCT Images

In order to create a 3D volume of the trachea from the OCT images, the images would have to be segmented between the trachea wall and the probe or air. Rather than manually segmenting each image which would involve a human looking through each individual image to determine what is a tracheal wall and what is not, a segmentation algorithm was applied to create segmented images of each OCT image. The segmentation starts with de-noising where a median filter is applied to the image to reduce speckle noise. To reduce the reflection from the sheath, the summation of the pixel intensity in a single A line is calculated. The wall is recognized by binarization, so the general outline of the tracheal wall is achieved. Small objects are removed, and then the tissue underneath is masked and de-emphasized so lumen detachment is not a concern [8].

For edge detection, a technique called dynamic programming was used. With i being the transverse direction and j being the vertical direction Eq.1 is as follows:

$$\begin{aligned} &\mathrm{Cost}(i,j) \\ &= \min \begin{bmatrix} \lambda \cdot w(I(i-1,j+1),I(i,j)) + \mathrm{Cost}(i-1,j+1), \\ w(I(i-1,j),I(i,j)) + \mathrm{Cost}(i-1,j), \\ \lambda \cdot w(I(i-1,j-1),I(i,j)) + \mathrm{Cost}(i-1,j-1) \end{bmatrix} \\ &= \min \begin{bmatrix} \cos t_1, \\ \cos t_2, \\ \cos t_3 \end{bmatrix} \end{aligned} \tag{1}$$

The image is given as a set of intensity values: a cost value is assigned to each node which in this case would be pixels. The image is then divided into columns where the minimum cost values of each column are used to create the shortest path from the first to the last column. The segments frames were then taken and placed 0.2mm away from each other in order to create the 3D volume (fig 4). The model is the trachea from the carina to the epiglottis: 150 frames were used for the reconstruction of each trachea with the length of each trachea being about 3 cm on average for all groups of rats used in this study [8].

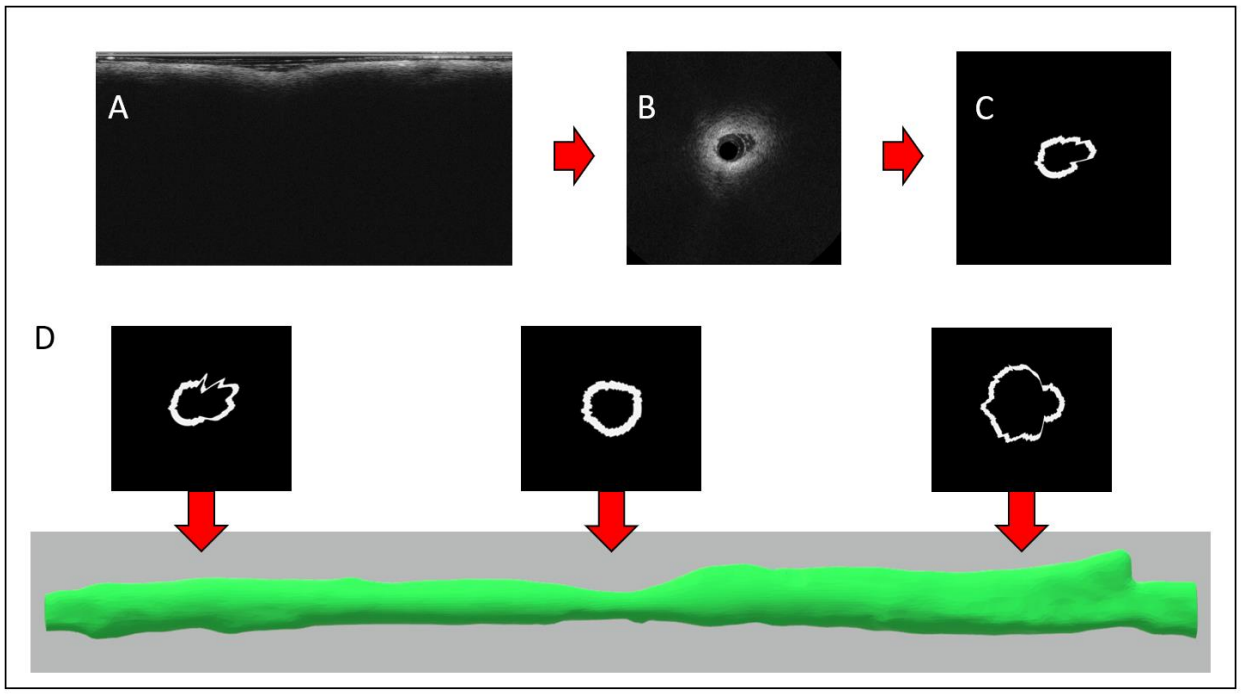

Figure 4 – A. Picture of the initial OCT image gathered by using a rotating probe. B. The image is then reconstructed to give the cross-sectional view. C. The image after it has been segmented using the dynamic programming algorithm. D. Using the many segmented images as the frames that would be used to reconstruct the airway as a 3D volume.

2.3 Preparing Model for Simulation

To prepare the model for ANSYS CFD, a clearly defined inlet and outlet needed to be created as a starting point for the air to move in and out of the trachea. The models were loaded into Meshlabs to reduce the geometry complexity and to reduce computation times [9]. The inlet and outlet were created in SolidWorks by cutting the ends of the model to create a flat face (fig 5). This was done so that the flow would start at a single, even planed face instead of many smaller irregular faces. ANSYS needed to create its own mesh to perform the simulation and required some definitions. The inlet, outlet, fluid zone, and walls of the model were defined for the program to understand what it was simulating. In this case the model imported from SolidWorks was the air that would be moving through the trachea with the walls acting as the trachea layer that was in contact with the air. Cells were generated by ANSYS to smooth out the

mesh generated and reduce computation load (fig 6). Body sizing was also used to keep element sizes from going below 1e-03 mm to reduce computational load, and inflation was used to create a finer mesh at the walls of the model to give more accurate results (fig 7).

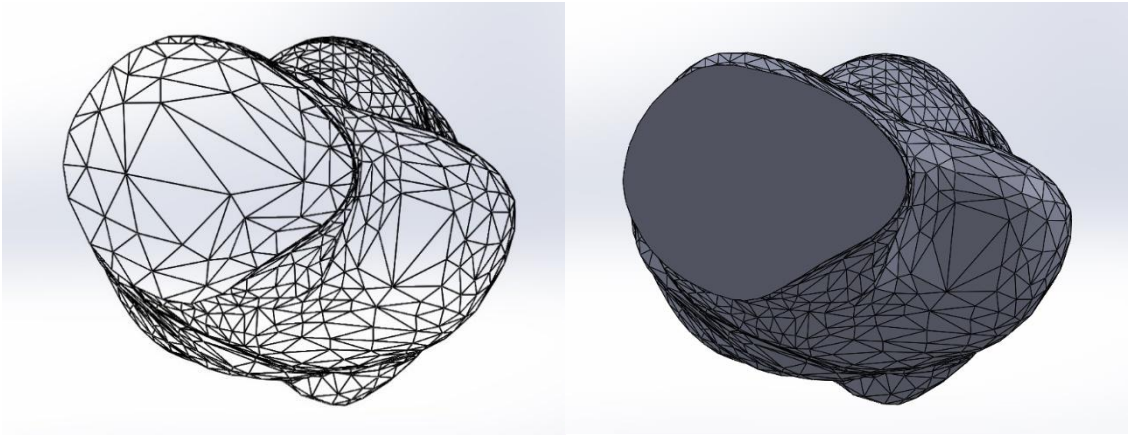

Figure 5 -The left image is the model created using the 3D reconstruction algorithm with multiple small faces that would each individually have to be given a starting condition; the right image is after the ends are cut to create a flat surface for use with ANSYS allowing the use of a single, uniform starting value.

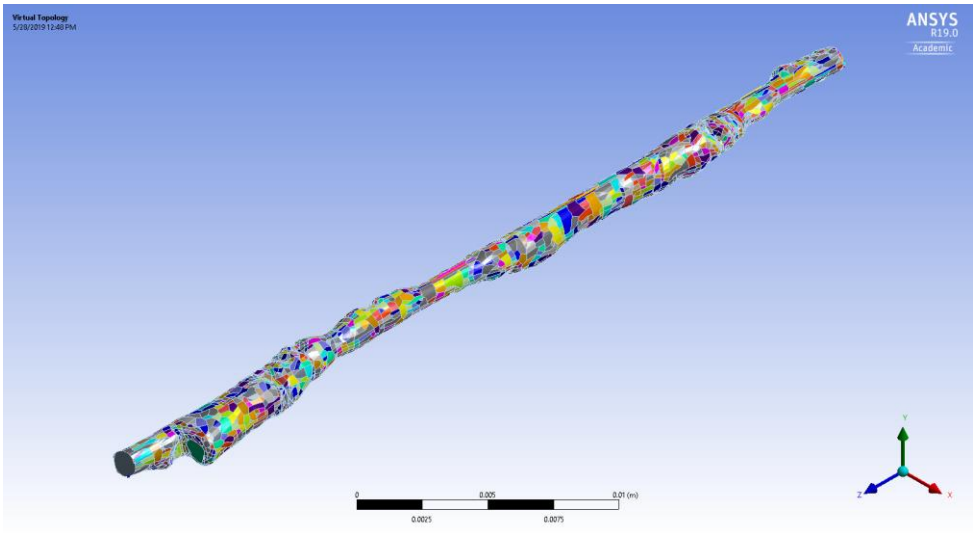

Figure 6 - The model after ANSYS has generated cells from the faces of the model to reduce computation time and allow for a smoother model.

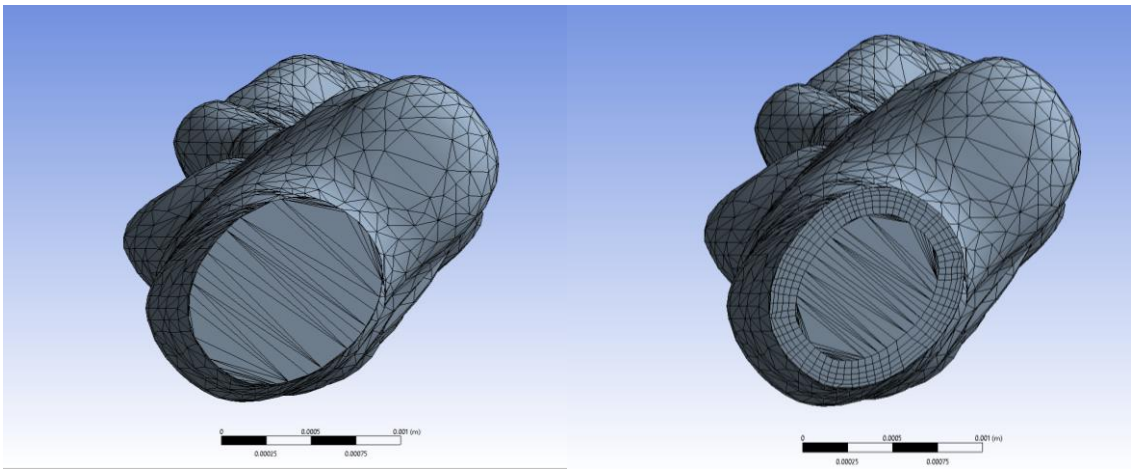

Figure 7 - The left image is the model before inflation. Right image shows the model after inflation. There is a tree ring like pattern bordering the walls and a higher density of the faces.

2.4 Turbulent vs. Laminar Flow

A laminar simulation using ANSYS Fluent was first used to determine whether the model would reach a Reynold's number that would suggest turbulence or if a laminar simulation would provide enough results for this situation. A starting airflow of 2.58 cc/s was used for each rat with the assumption that the rat would have tried to keep the same airflow despite narrowing of the airways [10]. Although ANSYS requires a starting velocity for its initial conditions, airflow was chosen so that each rat would have the same volume of air move through the trachea. To calculate the starting velocity (V) the airflow (Q) was divided by the inlet cross-sectional area (A) Eq.2.:

$$Q = VA \tag{2}$$

The velocity was used to calculate the Reynold's number with the viscosity of air and the characteristic diameter of the model being known Eq.3:

$$Re = \frac{vl}{\nu} \tag{3}$$

In the equation velocity (v) and characteristic dimension (l) are divided by viscosity (ν) which in this case is air. The characteristic dimension was calculated by using the area of the inlet and pie to determine what the diameter of the irregular circle is. If the simulation gave a Reynold's of 2000 or over, then it would be considered turbulent, but after running each simulation once as laminar, the Reynold's number for each model never exceeded 200 so the simulations were kept as laminar (fig 9) [11]. Once the simulations were completed, the velocity and pressure data were extracted from 40 frames evenly spaced out across the model (fig 10). To get the airway resistance, the difference between two frames was taken, and then the average flow rate was computed.

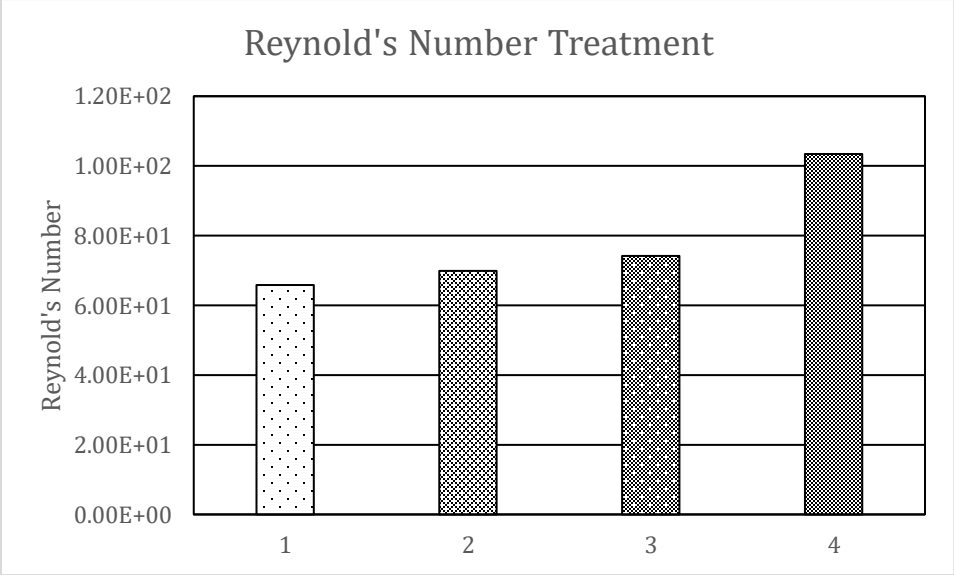

Figure 8- The graph shows the average Reynold's number of each group. 1 is the 30mg NO_2OA group; 2 is the 15mg NA_2OA group; 3 is the Oleic Acid Group; and 4 is the MIC group. While the MIC does show the highest Reynold's compared to the other groups, the numbers do not come close to the 2000 threshold needed to consider turbulence.

2.5 Assumptions and Model Parameters

For the model, assumptions had to be made about its physical properties in order for the simulation to be performed. The trachea is a living tissue with its own physical properties, but for

the purposes of these simulations, the model was assumed to be a rigid body. This was done to reduce computational times and reduce the resources needed for each simulation. The other assumption made was that each rat would breathe at the same volumetric flow rate despite some rats having narrowing occurring at the trachea. The rat in the simulation was assumed to try to breathe the same volume of air a healthy rat would breathe.

For laminar flow simulations in ANSYS Fluent, the two governing equations are the mass conservation equation which is the general form of the mass conservation Eq.4 except the S_m is a user defined value that the program starts with:

$$\frac{\partial \rho}{\partial t} + \nabla \cdot (\rho \vec{v}) = S_m \tag{4}$$

The other equation ANSYS uses is the momentum conservation equation Eq.5:

$$\frac{\partial}{\partial t}(\rho \vec{v}) + \nabla \cdot (\rho \vec{v} \vec{v}) = -\nabla p + \nabla \cdot (\bar{\bar{\tau}}) + \rho \vec{g} + \vec{F}$$

$$\bar{\bar{\tau}} = \mu \left[(\nabla \vec{v} + \nabla \vec{v}^{\,\mathrm{T}}) - \frac{2}{3} \nabla \cdot \vec{v} I \right]$$

For the variables p is the static pressure, $\bar{\bar{\tau}}$ is the stress tensor, pg and F are gravitation body forces with F being the model user defined source terms. For the stress tensor term, μ is the molecular viscosity, I is the unit tensor, and the second term on the right hand side is the effect of volume dilation. No mixing, heat transfer, or compressibility were needed for this simulation, so those equations are not relevant [12].

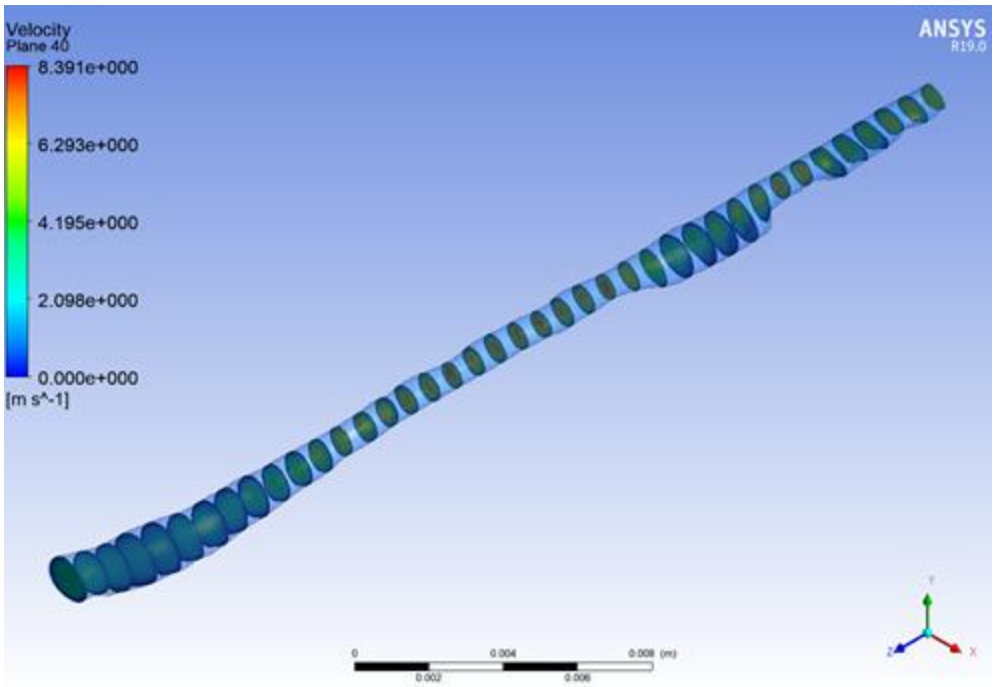

Figure 9 - Image of model after being divided into 40 different frames that were used to extract data.

3. RESULTS AND DISCUSSION

3.1 Cross-sectional Area of Trachea

When comparing the four groups, the MIC only rats performed worse in every regard. Physiologically, the MIC rats had a much lower cross-sectional area when compared to the other groups. The MIC treated rats had a CSA of only 5.38 ± 1.05 mm^2 while the 30mg NO_2OA, 15mg NO_2OA and Oleic Acid group showed 9.01 ± 0.49, 8,20, and 7.22 mm^2, respectively (fig 11). Due to the lower cross-sectional area when compared to the NO_2OA treated rats, the velocity and pressure drop across the trachea were much higher which led to an increase in airway resistance.

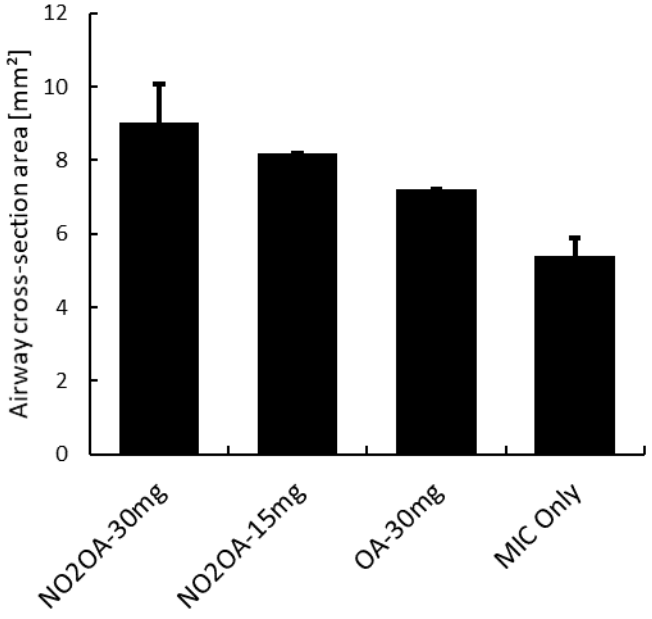

Figure 10 - A graph showing the difference in cross-sectional areas of each group of rat tracheas. MIC shows the lowest area while the 30mg NO_2OA group shows the highest.

3.2 Velocity Across Rat Trachea

Looking at the velocity of air across the tracheas, the 30mg NO_2OA group had an average of 0.968 ± 0.322 m/s, the 15 mg NO_2OA group had a velocity of 1.03 m/s, the Oleic Acid group

had a velocity of 1.11 m/s, and the MIC only group had an average velocity of 2.01 ± 0.144 m/s. When comparing the 30mg NO_2OA group averages with the MIC group, the MIC velocity was 107.6% higher than the 30 mg NO_2OA group (fig 12). With a t-test, a p-value of 0.9545 was achieved meaning the two data sets do not have similar means. All the tracheas behaved as expected with the center region having the highest velocity while the walls of the model were much lower. The simulations behaved as expected with the smaller cross-sectional areas having a higher velocity.

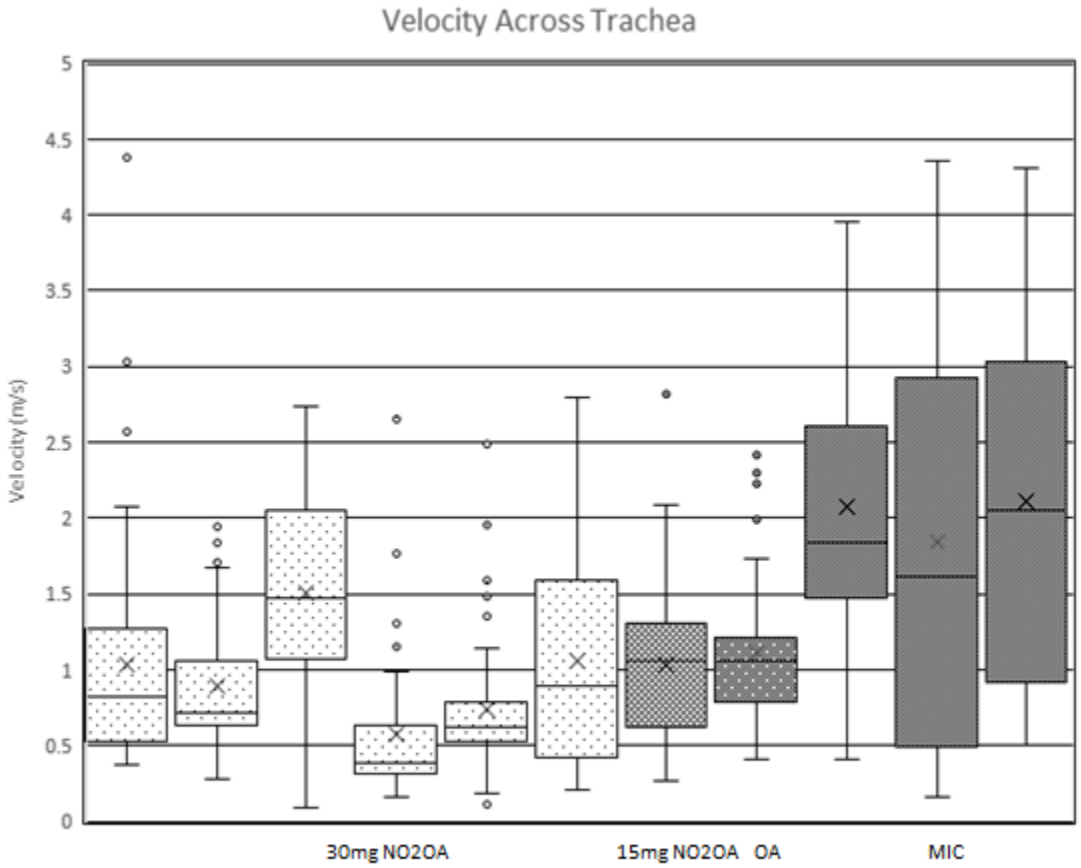

Figure 11 - Graph of the average velocity of air across each trachea that was used in the experiment. MIC group showed the highest velocities.

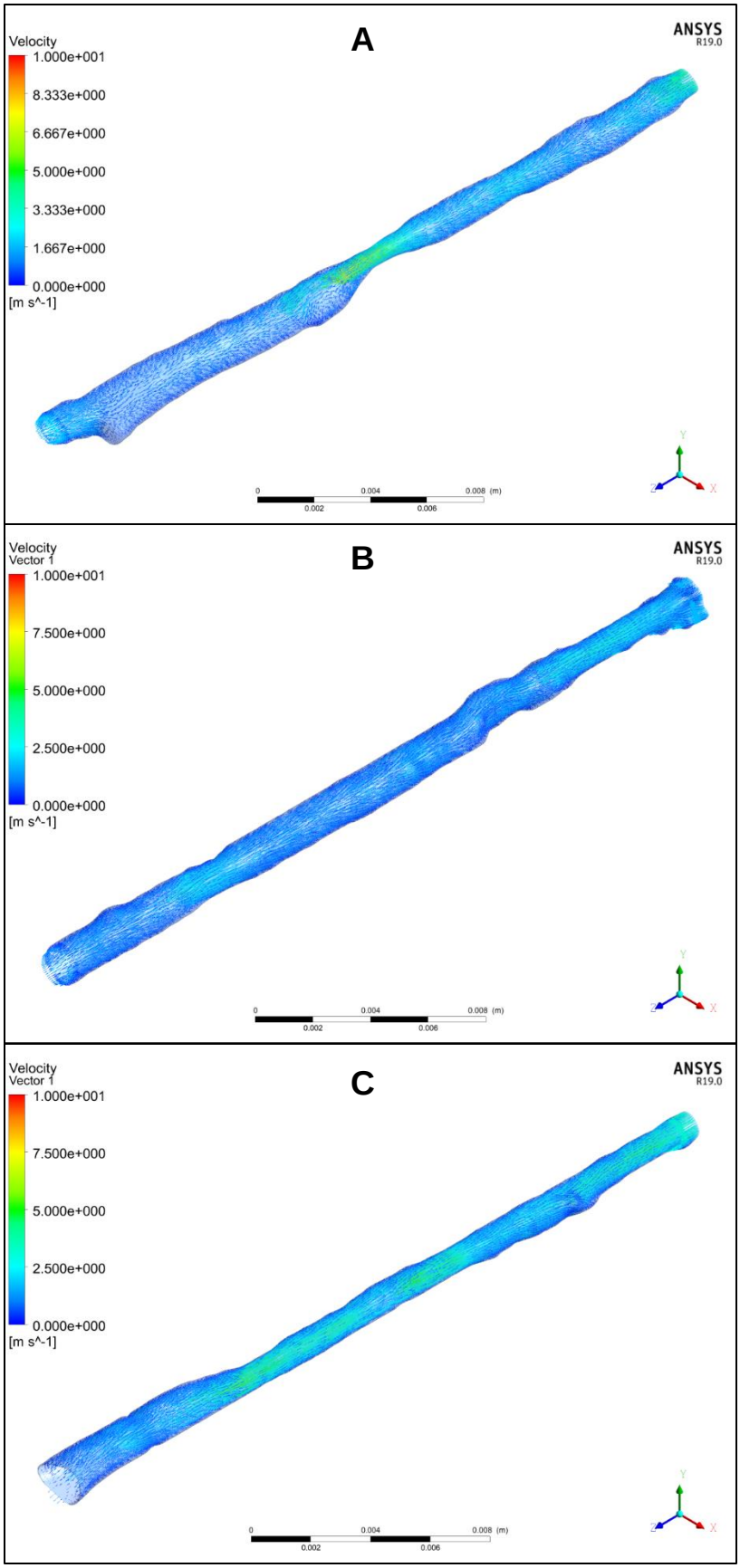
A
Velocity
1.000e+001
8.333e+000
6.667e+000
5.000e+000
3.333e+000
1.667e+000
0.000e+000
[m s^-1]
ANSYS
R19.0
0
0.004
0.008 (m)
0.002
0.006
B
Velocity
Vector 1
1.000e+001
7.500e+000
5.000e+000
2.500e+000
0.000e+000
[m s^-1]
ANSYS
R19.0
0
0.004
0.008 (m)
0.002
0.006
C
Velocity
Vector 1
1.000e+001
7.500e+000
5.000e+000
2.500e+000
0.000e+000
[m s^-1]
ANSYS
R19.0
0
0.004
0.008 (m)
0.002
0.006

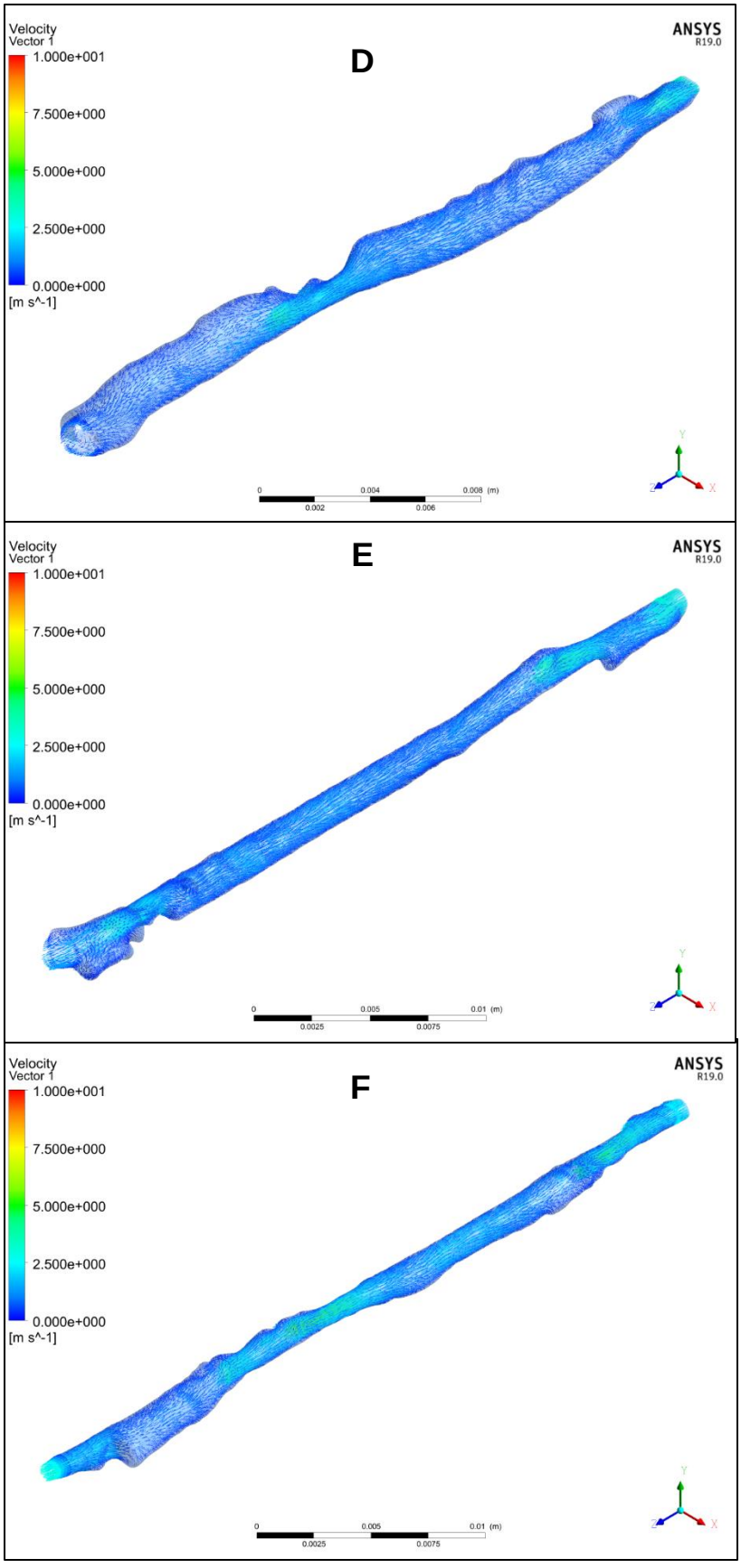
Velocity
Vector 1
1.000e+001
7.500e+000
5.000e+000
2.500e+000
0.000e+000
[m s^-1]
D
ANSYS
R19.0
0
0.004
0.008 (m)
0.002
0.006
Velocity
Vector 1
1.000e+001
7.500e+000
5.000e+000
2.500e+000
0.000e+000
[m s^-1]
E
ANSYS
R19.0
0
0.005
0.01 (m)
0.0025
0.0075
Velocity
Vector 1
1.000e+001
7.500e+000
5.000e+000
2.500e+000
0.000e+000
[m s^-1]
F
ANSYS
R19.0
0
0.005
0.01 (m)
0.0025
0.0075

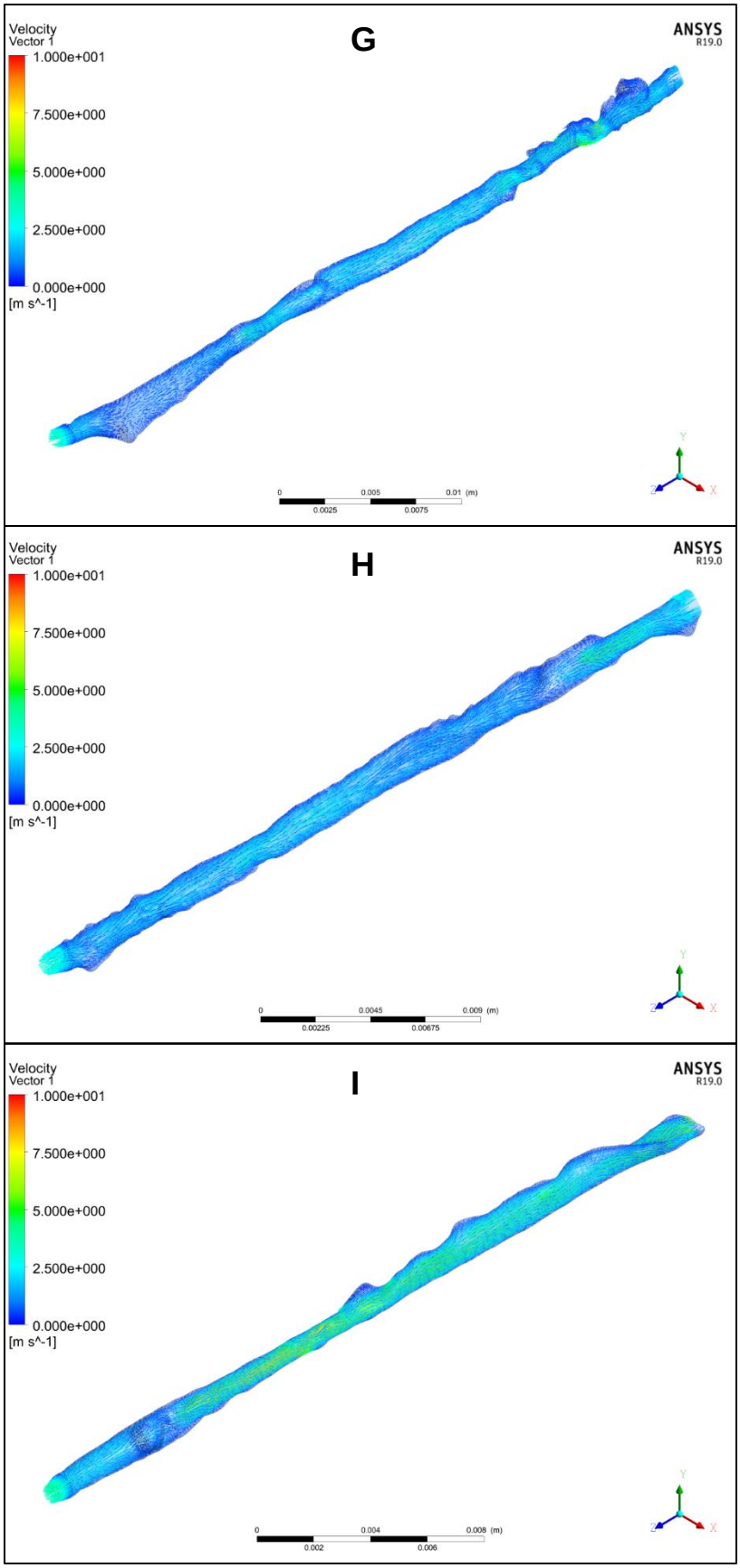
Velocity
Vector 1
1.000e+001
7.500e+000
5.000e+000
2.500e+000
0.000e+000
[m s^-1]
G
ANSYS
R19.0
0
0.005
0.01 (m)
0.0025
0.0075
Velocity
Vector 1
1.000e+001
7.500e+000
5.000e+000
2.500e+000
0.000e+000
[m s^-1]
H
ANSYS
R19.0
0
0.0045
0.009 (m)
0.00225
0.00675
Velocity
Vector 1
1.000e+001
7.500e+000
5.000e+000
2.500e+000
0.000e+000
[m s^-1]
I
ANSYS
R19.0
0
0.004
0.008 (m)
0.002
0.006

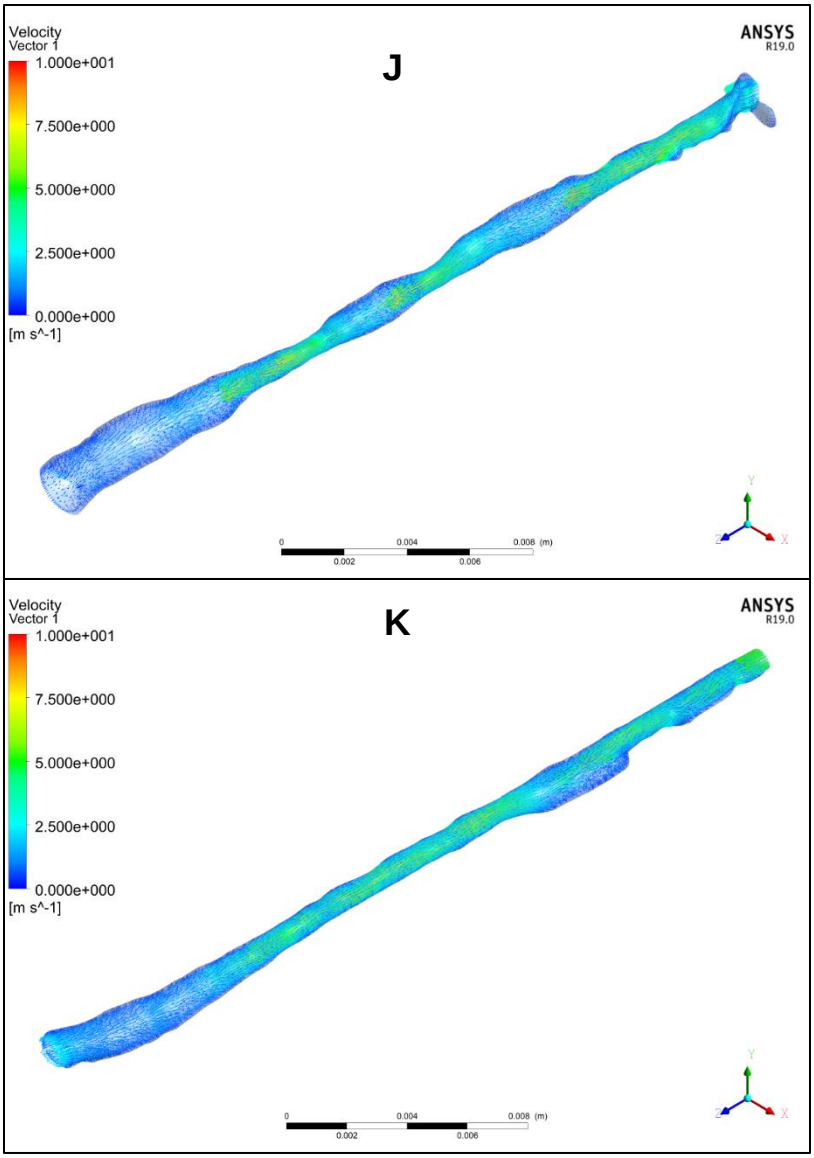

Figure 12- Velocity vector images of airway. Models A-E are the 30mg NO_2OA group; G is the 15mg NO_2OA group; H is the Oleic Acid Group; and I, J, K are the MIC group.

Looking at the models (fig 13), one of the features that stand out is that while the cross-sectional area on average has increased in the 30 mg NO_2OA group compared to the MIC group, there are still areas that have large stenosed areas. This may imply that the treatment was not applied properly, or there are possibly some at around the midpoint region of the trachea where the treatment was not very effective. This can be seen clearly in model A where the midpoint has a large stenosed region that causes the velocity to drastically increase when compared to the

other tracheas in the group. The velocity is more akin to the velocities found in the MIC group which could become a problem if left untreated. The Oleic acid group did not perform as expected from the cross-sectional analysis where it had a higher cross-sectional area on average compared to the NO_2OA group. The velocity across the trachea for the Oleic acid group did not resemble that of the MIC group.

3.3 Pressure Drop Across Rat Trachea

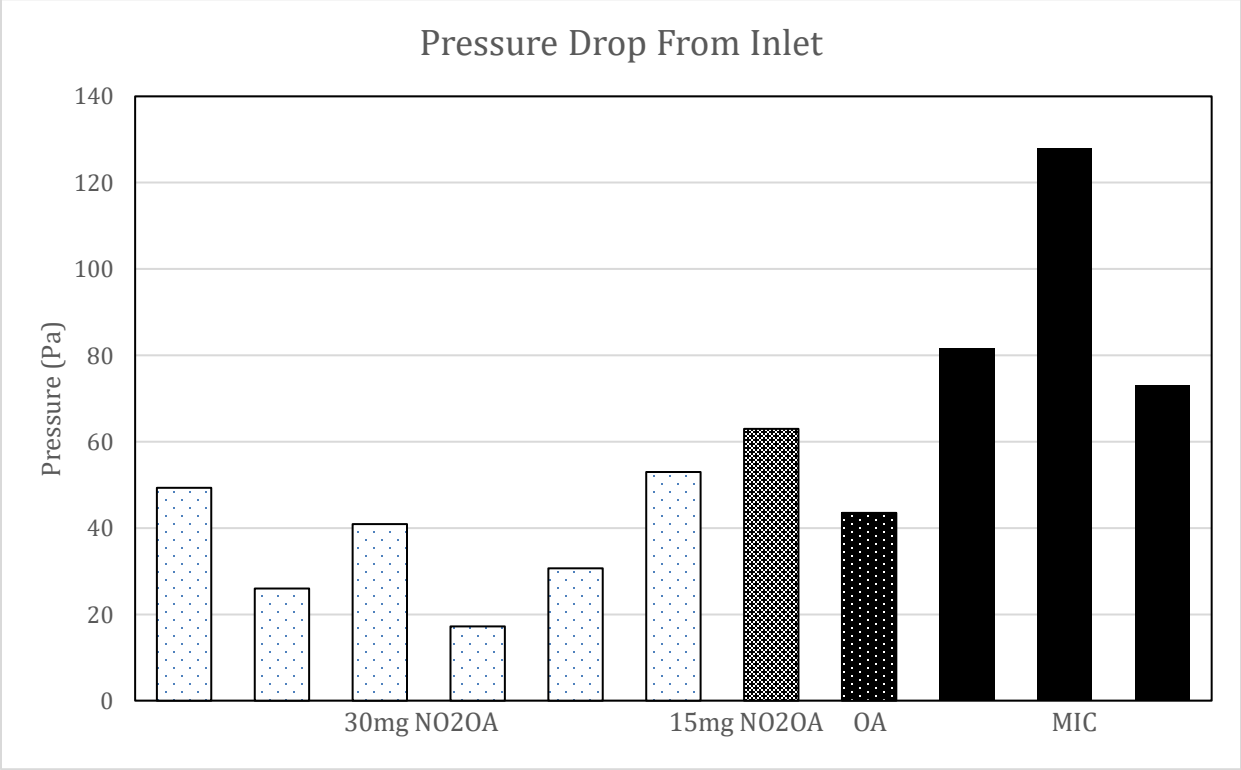

Figure 13 – Graph showing the pressure drop of each rat trachea. The MIC group has the highest pressure drops across the trachea while the 30mg group has the lowest on average.

The pressure was graphed as a difference from the pressure of one frame to another (Fig. 11). The 30mg NO_2OA group had relatively low changes in pressure except for one trachea having a spike in pressure change across the trachea (fig 14). The pressure drops also had similar patterns as the velocity with the 30mg NO_2OA group having an average of 1.125 ± 0.589 pa drop per frame; the 15mg NO_2OA group had a 1.161 pa drop per frame, the Oleic Acid group

had a 0.786 pa drop per frame, and the MIC group had a 2.200 ± 0.742 pa drop per interframe volume. The average pressure drop for each group is 36.169 ± 13.938 pa for the 30mg NO_2OA group, 62.962 pa for the 15mg NO_2OA group, 43.498 pa for the OA group, and 94.202 ± 29.580 for the MIC group (fig 15). This matches with the velocity data in that the MIC rats performed the worst in terms of the parameter in the simulation. From the simulation, the rat would need a higher starting pressure in order to get the air to move down the trachea and into the lungs due to narrowing of the trachea.

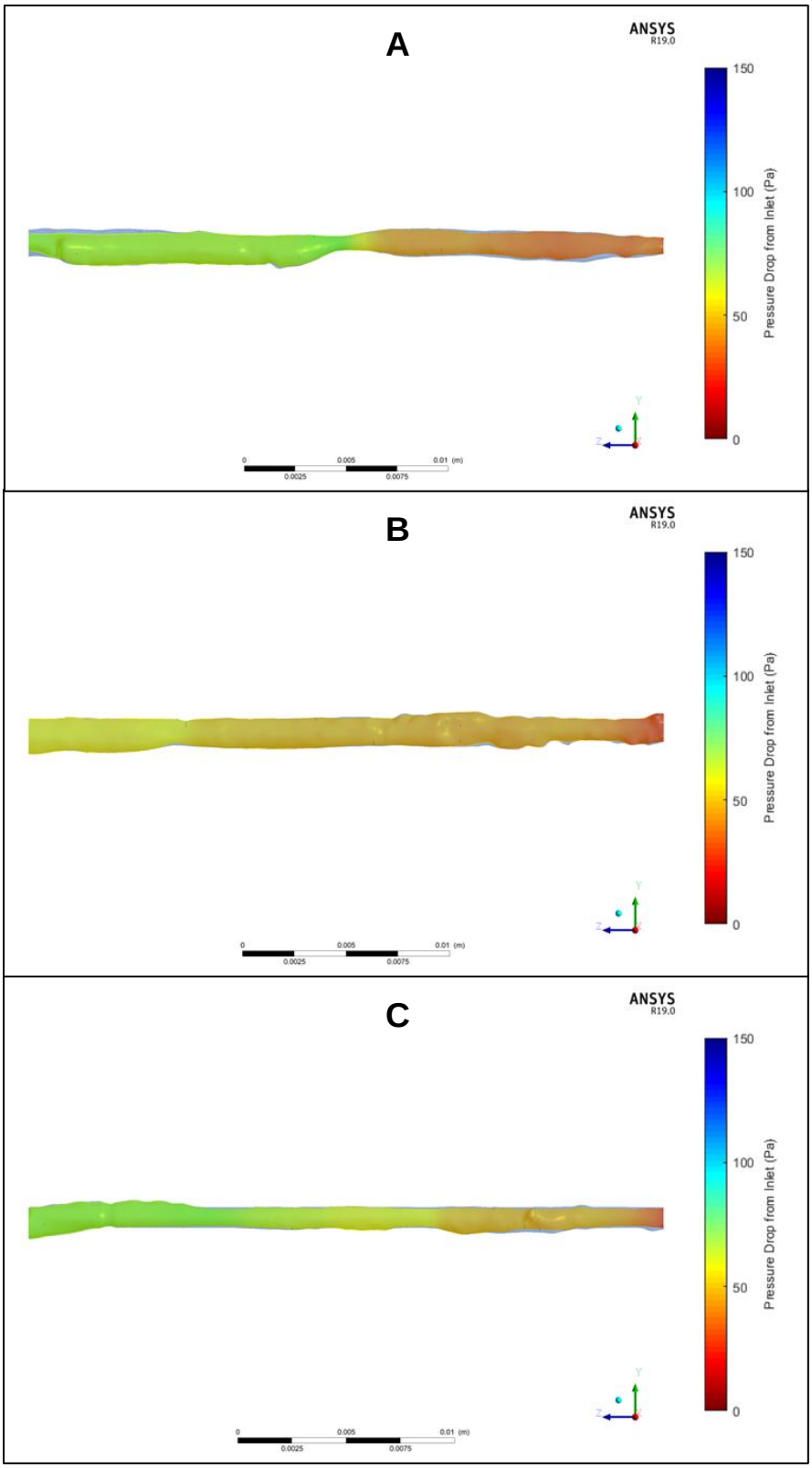
A
ANSYS
R19.0
150
100
50
0
Pressure Drop from Inlet (Pa)
0
0.005
0.01 (m)
0.0025
0.0075
B
ANSYS
R19.0
150
100
50
0
Pressure Drop from Inlet (Pa)
0
0.005
0.01 (m)
0.0025
0.0075
C
ANSYS
R19.0
150
100
50
0
Pressure Drop from Inlet (Pa)
0
0.005
0.01 (m)
0.0025
0.0075

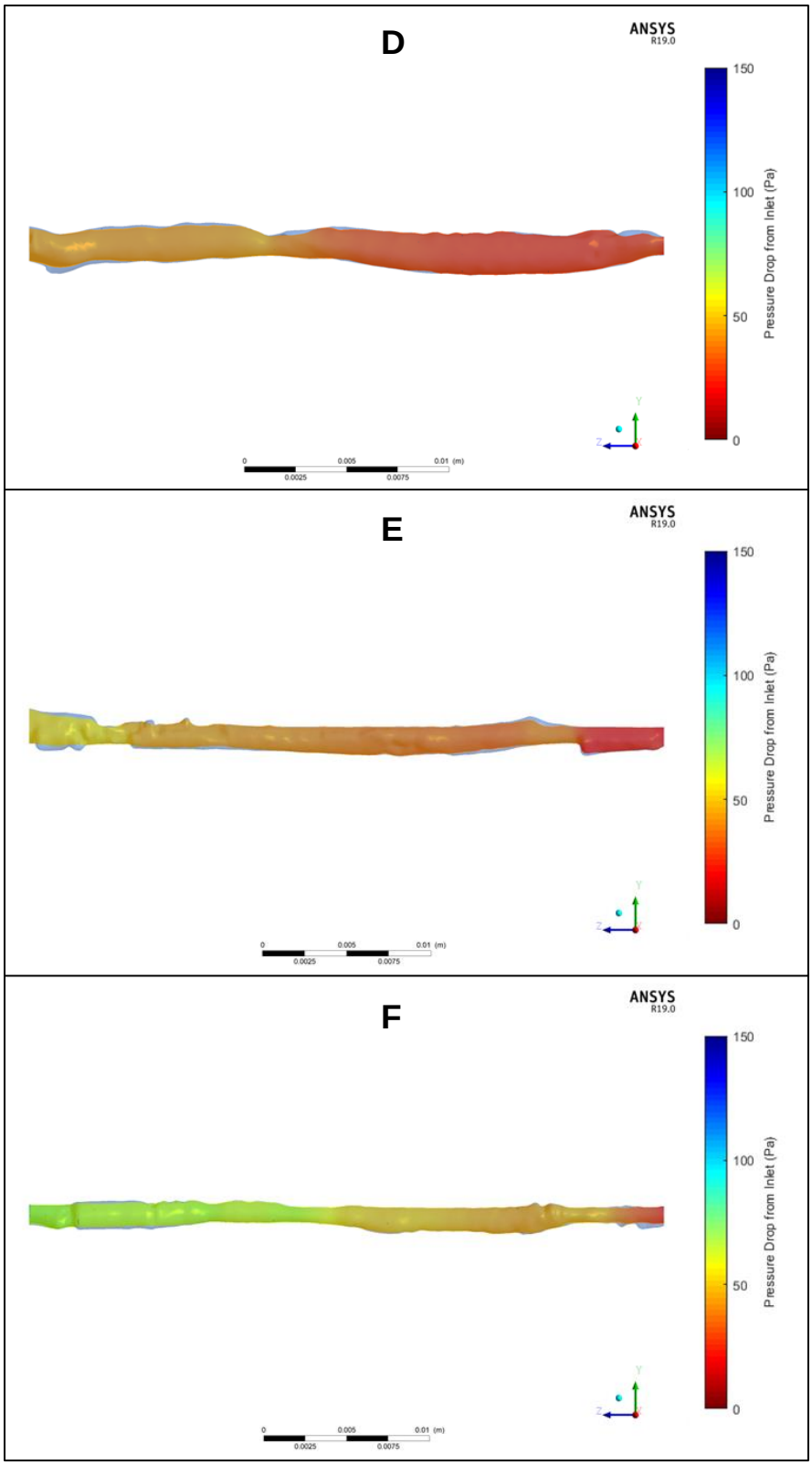
D
ANSYS
R19.0
150
100
50
0
Pressure Drop from Inlet (Pa)
0
0.005
0.01 (m)
0.0025
0.0075
E
ANSYS
R19.0
150
100
50
0
Pressure Drop from Inlet (Pa)
0
0.005
0.01 (m)
0.0025
0.0075
F
ANSYS
R19.0
150
100
50
0
Pressure Drop from Inlet (Pa)
0
0.005
0.01 (m)
0.0025
0.0075

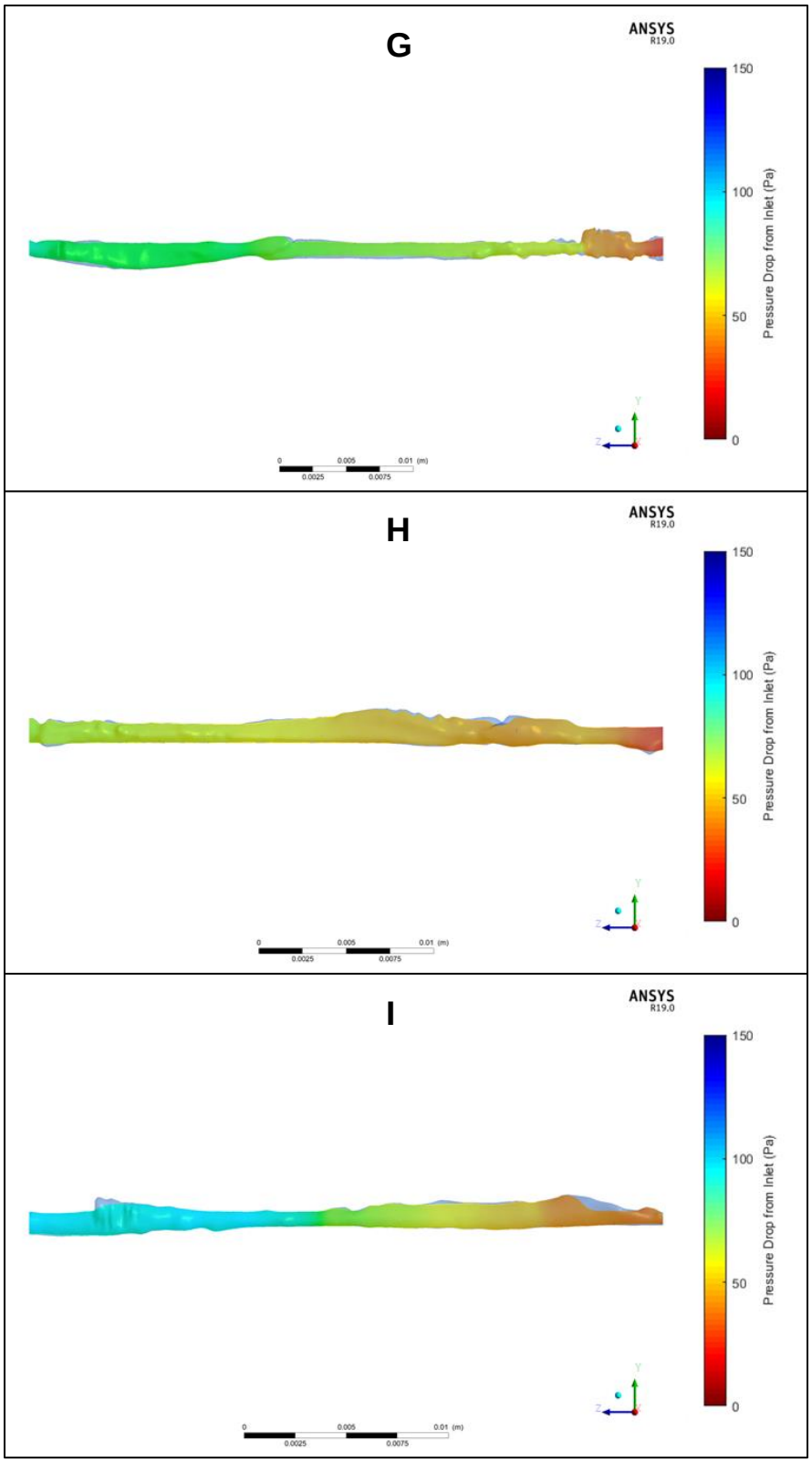
G
ANSYS
R19.0
150
100
50
0
Pressure Drop from Inlet (Pa)
0
0.005
0.01 (m)
0.0025
0.0075
H
ANSYS
R19.0
150
100
50
0
Pressure Drop from Inlet (Pa)
0
0.005
0.01 (m)
0.0025
0.0075
I
ANSYS
R19.0
150
100
50
0
Pressure Drop from Inlet (Pa)
0
0.005
0.01 (m)
0.0025
0.0075

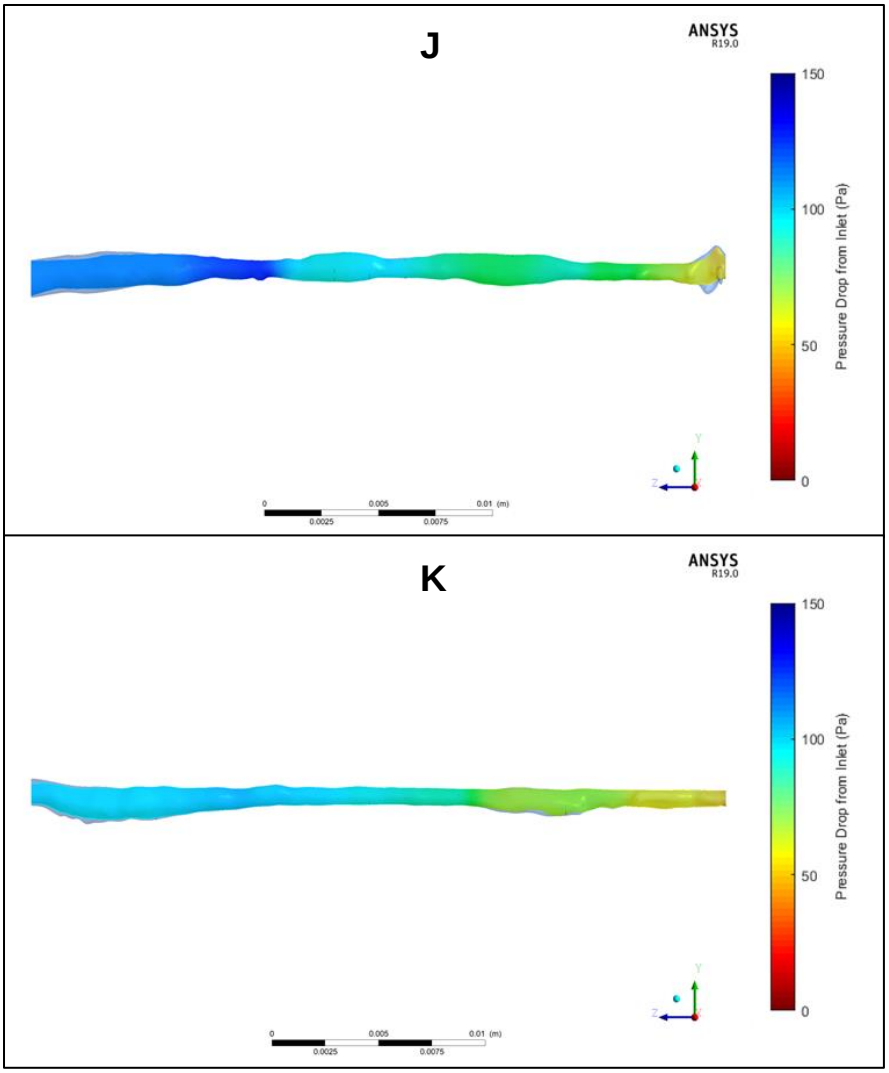

Figure 14- Pressure drop images across the airway. Models A-E are the 30mg NO_2OA group; G is the 15mg NO_2OA group; H is the Oleic Acid Group; and I, J, K are the MIC group. The color bar represents the difference in pressure at a location from the initial starting pressure at the inlet which is on the right-hand side.

3.4 Airway Resistance Across

In order to calculate the airway resistance, the volumetric air flow and the pressure changes across the trachea were needed with the equation being Eqn.6:

$$R_{AW} = \frac{\Delta P}{V} \tag{6}$$

with R_{AW} being the resistance, ΔPbeing the pressure drop and V being the volumetric airflow.

The airway resistance calculated from the flow rate and pressure drop also showed similar results to the velocity and pressure data. The 30mg NO_2OA group performed the best while the MIC group performed the worst. The 15mg NO_2OA group again did not perform as well as the 30mg group but did perform better than the MIC group. The average airway resistance for the 30mg NO_2OA and MIC group was 0.1436 ± 0.06 and 0.41 ± 0.0549 $\mathrm{cmH^2O} * \mathrm{s/ml}$, respectively. Using these two values, there was a 184.5% increase in airway resistance depending on the group the trachea came from.

When comparing the simulation results, the data is similar to what other groups have determined from fluid simulations. Jinxiang Xi et al. showed a velocity of approximately 4 m/s at the fastest regions in the trachea of a healthy rat and a pressure drop of approximately 50 Pa [13]. Corely et al. also produced similar results with the air velocity in the trachea reaching a maximum of 4~4.5 m/s inside a healthy rat trachea [14]. These values are in line with the 30mg NO_2OA group while the MIC group shows about double to triple the values of what would be

considered healthy from the other groups' data.

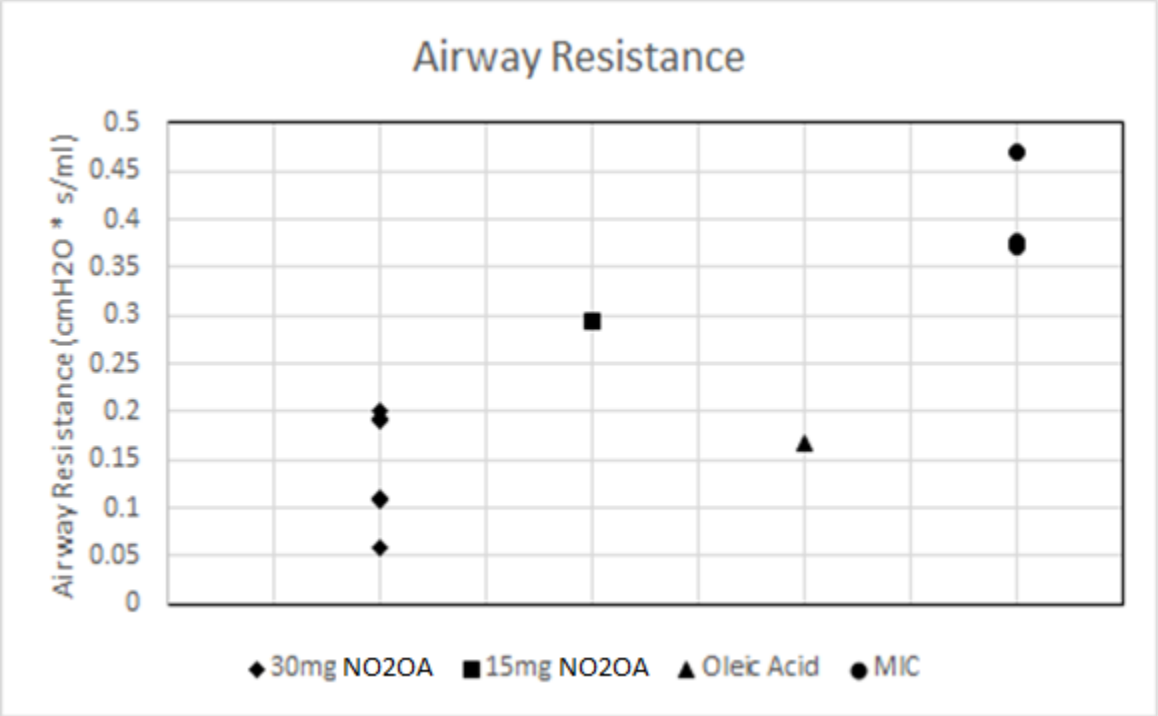

Figure 15 - Air resistance of each trachea based on groups. Again, MIC is the highest while the 30mg NO_2OA group averages the lowest.

4. CONCLUSION AND FUTURE WORK

One of the major limitations of this study was the lack of *in vivo* images that could be used for 3D reconstruction. All the images were taken of mounted rat tracheas that were attached to the rat after being euthanized. The area of the trachea changes after the rat has been euthanized. Then there is also further change due to the mounting of the tracheas so that they can be shipped and imaged at a different location. The rat would also have changes in the cross-sectional area from breathing in and out. To fix these issues, the first step would be to image a living rat that has inhaled the gas and image another that has been treated. Nothing about the current system requires the rat to be euthanized beforehand in order to image the trachea. Once the mouse is anesthetized, the breathing artifacts should be minimal, and the same method used before on the mounted tracheas should still work on the new in vivo rats.

Another limitation was the number of samples for the 15mg NO_2OA and the Oleic Acid groups. For this study, there was only one trachea for the 15mg NO_2OA group and one trachea for the Oleic Acid group which did not behave as expected. Ideally, the Oleic acid rat trachea would mimic the characteristics of the MIC rat tracheas but what was found did not match that assumption. With a single sample, it cannot be definitively determined if the placebo was effective. Ideally in a future study, the sample sizes of each group would be increased in order to determine the full effect of NO_2OA treatment. There could also be an increased number of groups to see if there is a linear relation between airway resistance and NO_2OA used. NO_2OA may also have an upper threshold where increasing the dosage per treatment would not improve the outcome of the tracheal wall repair.

Another major limitation of the study is the wall properties of the trachea during the simulations. The trachea is normally living tissue with many different mechanical properties. It

would also slightly change in terms of area during the breathing in and out motions which were not accounted for in this model. The model may not be that much more accurate due to the trachea being a static structure so changing those parameters may not be worth the increased computational time.

What these simulations have shown is that there is a decrease on average in airway resistance of the NO_2OA treated group when compared to the MIC only group. Beyond the simulation work, the images could also be used by a physician in order to determine if the drug was properly applied. Looking at the NO_2OA treated groups, while on average the cross-sectional area has increased, some of the tracheas still show pinched areas that significantly increase airway resistance across the trachea. Using these models, the physician could reapply NO_2OA on areas that seem to still be suffering from epithelium collapse.

REFERENCES

1. Mehta, P. S., Mehta, A. S., Mehta, S. J. & Makhijani, A. B. Bhopal Tragedy's Health Effects: A Review of Methyl Isocyanate Toxicity. *JAMA* 264, 2781–2787 (1990).
2. Tice, R. R., Luke, C. A. & Shelby, M. D. Methyl isocyanate: An evaluation of in vivo cytogenetic activity. *Environmental Mutagenesis* 9, 37–58 (1987).
3. Zhang Jifeng *et al.* Nitro-Oleic Acid Inhibits Angiotensin II–Induced Hypertension. *Circulation Research* 107, 540–548 (2010).
4. D'Amore, A. *et al.* Nitro-Oleic Acid (NO(2)-OA) Release Enhances Regional Angiogenesis in a Rat Abdominal Wall Defect Model. *Tissue Eng Part A* 24, 889–904 (2018).
5. Elbau, P., Mindrinos, L. & Scherzer, O. Mathematical Methods of Optical Coherence Tomography. in *Handbook of Mathematical Methods in Imaging* (ed. Scherzer, O.) 1169–1204 (Springer New York, 2015). doi:10.1007/978-1-4939-0790-8_44
6. Rancourt, R. C. *et al.* Methyl isocyanate inhalation induces tissue factor-dependent activation of coagulation in rats. *Drug and Chemical Toxicology* **42**, 321–327 (2019).
7. Miao, Y. *et al.* Automated 3D segmentation of methyl isocyanate-exposed rat trachea using an ultra-thin, fully fiber optic optical coherence endoscopic probe. *Scientific Reports* 8, 8713 (2018).
8. Qi, L. *et al.* Automatic airway wall segmentation and thickness measurement for long-range optical coherence tomography images. *Opt Express* 23, 33992–34006 (2015).
9. P. Cignoni, M. Callieri, M. Corsini, M. Dellepiane, F. Ganovelli, G. Ranzuglia. MeshLab: an Open-Source Mesh Processing Tool. Sixth Eurographics Italian Chapter Conference, page 129-136, 2008

10. Minard, K. R. *et al.* Phase-contrast MRI and CFD modeling of apparent ^{3}He gas flow in rat pulmonary airways. *J Magn Reson* 221, 129–138 (2012).
11. Kim, J., Moin, P. & Moser, R. Turbulence statistics in fully developed channel flow at low Reynolds number. *Journal of Fluid Mechanics* 177, 133–166 (1987).
12. Batchelor, G. K. *An Introduction to Fluid Dynamics*. (Cambridge University Press, 2000). doi:10.1017/CBO9780511800955
13. Xi, J., Hu, Q., Zhao, L. & Si, X. A. Molecular Binding Contributes to Concentration Dependent Acrolein Deposition in Rat Upper Airways: CFD and Molecular Dynamics Analyses. *Int J Mol Sci* 19, 997 (2018).
14. Corley, R. A. *et al.* Comparative computational modeling of airflows and vapor dosimetry in the respiratory tracts of rat, monkey, and human. *Toxicol Sci* 128, 500–516 (2012).